Applied Surface Science 437 (2018) 202–208

Contents lists available at ScienceDirect

Applied Surface Science

journal homepage: www.elsevier.com/locate/apsusc

Full Length Article

# A significant reduction of ice adhesion on nanostructured surfaces that consist of an array of single-walled carbon nanotubes: A molecular dynamics simulation study

Luyao Bao[a], Zhaoyuan Huang[a], Nikolai V. Priezjev[b], Shaoqiang Chen[c], Kai Luo[a], Haibao Hu[a,d,*]

[a] School of Marine Science and Technology, Northwestern Polytechnical University, Xi'an, Shaanxi, 710072, PR China
[b] Department of Mechanical and Materials Engineering, Wright State University, Dayton, OH, 45435, USA
[c] Xi'an Precision Machinery Research Institute, Xi'an, Shaanxi 710075, PR China
[d] Research & Development Institute of Northwestern Polytechnical University in Shenzhen, Shenzhen, 518057, PR China

ARTICLE INFO

*Article history:*
Received 16 September 2017
Received in revised form
29 November 2017
Accepted 11 December 2017
Available online 12 December 2017

*Keywords:*
Ice adhesion reduction
Nanostructured surfaces
Molecular dynamics

ABSTRACT

It is well recognized that excessive ice accumulation at low-temperature conditions can cause significant damage to civil infrastructure. The passive anti-icing surfaces provide a promising solution to suppress ice nucleation and enhance ice removal. However, despite extensive efforts, it remains a challenge to design anti-icing surfaces with low ice adhesion. Using all-atom molecular dynamics (MD) simulations, we show that surfaces with single-walled carbon nanotube array (CNTA) significantly reduce ice adhesion due to the extremely low solid areal fraction. It was found that the CNTA surface exhibits up to a 45% decrease in the ice adhesion strength in comparison with the atomically smooth graphene surface. The details of the ice detachment from the CNTA surface were examined for different water-carbon interaction energies and temperatures of the ice cube. Remarkably, the results of MD simulations demonstrate that the ice detaching strength depends linearly on the ratio of the ice-surface interaction energy and the ice temperature. These results open the possibility for designing novel robust surfaces with low ice adhesion for passive anti-icing applications.



## 1. Introduction

The issue of excessive ice accumulation at low-temperature conditions poses a great challenge for infrastructure reliability and human security. For example, icy roads can easily cause car accidents and thus may raise the loss of life or personal injury [1,2]. The accretion of ice on airplane wings may result in reduced lift force and consequently tragic airplane crash [3]. In addition, glaze ice can significantly increase the weight of transmission lines and power network towers and lead to extensive damage to the infrastructure. For instance, severe snow storms hit South China and the northeastern United States, which left millions of people without power and led to billion-dollar economic losses in both countries [4,5]. Many other critical structures, such as buildings, bridges, wind turbines, and off-shore oil rigs, can also be damaged by the excessive weight of accumulated ice and stresses caused by freeze-thaw cycles [5,6]. Up to the present, extensive efforts have been made to understand the mechanism of icing and to develop efficient anti-icing techniques [4,5,7,8].

The traditional methods that are widely used at present can be categorized as *active* anti-icing methods, which include mechanical ice removal, active heating treatments, and chemical deicing. Often times, these methods are either expensive or environmentally unfriendly [7,9]. Thus, new technological solutions are needed. Recently, the *passive* anti-icing surfaces, or icephobic surfaces, have drawn increasing attention because of their significant economic, energy and safety implications in the icing proof and deicing [4,5]. The bio-inspired superhydrophobic surfaces (SHS) show promising potential to achieve the passive anti-icing properties [4,10,11]. The typical SHS combines the micro- and nanoscale structures and hydrophobic surface properties that result in large contact angles and small contact angle hysteresis of water droplets on SHS [12,13]. The so-called Cassie state [14] or fakir state [15] of a water droplet

* Corresponding author at: School of Marine Science and Technology, Northwestern Polytechnical University, Xi'an, Shaanxi, 710072, PR China.
*E-mail address:* huhaibao@nwpu.edu.cn (H. Hu).

https://doi.org/10.1016/j.apsusc.2017.12.096
0169-4332/

on a SHS is associated with a relatively small contact area between the surface of the water droplet and the solid areal fraction of the SHS.

The topographical features of the SHS minimize the interaction between the water droplet and the solid surface leading to unusual behavior; namely, the water droplet slides easily on the SHS [16,17] or it rebounds after the impact with the SHS [18]. Consequently, water droplets can be readily removed from the SHS before freezing [19]. Moreover, at low-temperature conditions, the ice formed on the SHS exhibits low adhesion, and, hence, it is also removed more easily [20–23]. In turn, the incorporation of re-entrant [24,25] and in some cases double re-entrant [26] curvatures into the microscopic texture of SHS can significantly improve the robustness of the repellent properties. The ability of anti-icing of SHS relies on its water wettability, and a number of recent studies have been carried out to correlate the ice adhesion and water wettability [27,28]. However, one of the major drawbacks of the SHS is lack of durability, i.e., the microstructures of SHS tend to be permanently damaged by ice removal and freeze-thaw cycles [29–32]. Thus, for challenging anti-icing applications, more advanced methods are required for large-scale fabrication of robust, passive anti-icing surfaces.

In this paper, we first show that surfaces with single-walled carbon nanotube array (CNTA) significantly reduce ice adhesion. Using all-atom molecular dynamics (MD) simulations, we demonstrate that the CNTA surface exhibits up to about 45% decrease in the ice adhesion strength in comparison with the atomically smooth graphene (SG) surface. The process of ice detachment from the CNTA and SG surfaces is investigated by adapting the water-carbon interaction potential and including the effect of temperature of the ice cube. We find that the ice detachment stress depends linearly on the ratio of the water-carbon interaction energy and temperature of the ice cube for both the CNTA and SG surfaces. We further comment that the CNTA surface has recently been manufactured by Zhang et al. through growing single-walled carbon nanotubes from the surfaces of solid carbide by controlling the symmetries of the active catalyst surface [33]. Thus, recent experimental studies and our atomistic simulation results open the possibility for designing novel, robust surfaces with low ice adhesion for passive anti-icing.

The paper is organized as follows. The details of MD simulations are given in the next section. The ice detachment process from CNTA and SG surfaces is examined in Section 3.1. The correlation between the ice adhesion strength and substrate-ice interaction (SII) energies for different temperatures is described in Section 3.2. The universal dependence of the ice adhesion strength on the SII energy and temperature is presented in Section 3.3. The summary is provided in the last section.

## 2. Details of MD simulations

In this section, we present the details of MD simulations used to study the detachment process of a nanoscale ice cube from SG and CNTA surfaces. The water model, TIP4P/Ice, was chosen to simulate the ice cube. We used the interaction parameters from the study by Abascal et al. [34] to simulate oxygen and hydrogen atoms and water molecules. This model was designed to reproduce the solid-phase properties of ice and it can predict accurately the melting temperature of hexagonal ice (272.2 K at 1 bar) without affecting the rest of the physical properties. Thus, this model is suitable for investigation of the ice detachment from solid substrates considered in our study. The bond lengths and bond angles of water molecules were also kept fixed using the SHAKE algorithm [35].

The ice Ih phase was considered in our study due to its ubiquity in nature [36]. The ice cube was constructed out of 5760 water molecules that form a hexagonal lattice with a basal face of (0 0 0 1) and surface area of $A$=7.2 × 7.0 nm$^2$ [see Fig. 1(a)]. The thickness of the ice cube is 3.5 nm. The (0 0 0 1) face of the ice cube was placed in contact with the substrates. In our setup, the SG surface is a single-layer graphene that consists of 5510 atoms with a surface area of 11.4 × 12.0 nm$^2$. The CNTA surface was constructed by introducing an array of single-walled carbon nanotubes (SWNT) on the SG surface. The SWNT has a length of 2.3 nm and chiral indices of (6, 6) and it is constructed using 240 atoms. The separation distance between centers of adjacent SWNTs is 1.02 nm in both $x$- and $y$-directions. The periodic boundary conditions were imposed along the $x$-, $y$- and $z$-directions. The surface areas of two substrates were chosen to be large enough in order to allow migration of the ice cube on substrates. The dimensions of the simulation domain were set to ensure that atoms of the ice cube do not interact with their periodic mirror images.

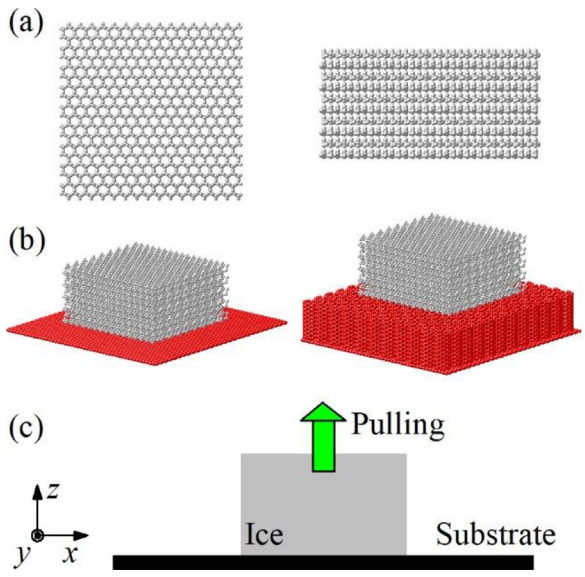


**Fig. 1.** Deicing models in MD simulations. (a) The ice block with the hexagonal arrangement of water molecules and a basal face (0 0 0 1). The left and right images are the top and side views, respectively. (b) The ice cube in contact with a smooth graphene solid substrate (left) and a substrate with the vertical single-walled carbon nanotube array (CNTA) (right). (c) Illustration of the detachment procedure used in MD simulations with increasing pulling force acting on the ice cube.

For simplicity, the atoms of CNTA and SG surfaces in the present study are electrically neutral and they do not interact with each other. Similar assumptions were also used in the previous ice detachment study [37] and wetting studies [38,39] using MD simulations. The interaction between the ice and substrates was modeled using the van der Waals interactions, i.e., the Lennard-Jones (LJ) potential between water molecules and substrate atoms. Note that the interaction parameters of the LJ potential between oxygen and carbon atoms vary in the published literature. We addressed this problem as follows. On the one hand, following the previous study [40], we choose the water-carbon LJ potential parameters that can reproduce experimentally observed contact angle of water on a clean graphitic surface [41]. More specifically, the characteristic length and energy for the LJ potential between oxygen and carbon atoms are $\sigma_{CO}$ = 3.19Å and $\varepsilon_{CO}$ = 0.4736 kJ/mol, respectively. In our setup, there is no interaction between hydrogen and carbon atoms. These interaction parameters between the substrate and water molecules were chosen to compare the strength of ice adhesion on the CNTA and SG surfaces. On the other hand, we varied the characteristic energy of the LJ potential between oxygen and carbon atoms, $\varepsilon_{CO}$, to cover values of parameters of the LJ potential used in other studies [37,40,42,43]. Meanwhile, the correlation between the ice adhesion strength and wettability can also be investigated since the substrate wettability depends sensitively

on the interaction energy, $\varepsilon_{CO}$ [42]. We leave the influence of electrostatic forces of the substrate on ice to future studies due to the highly complex situation with Coulombic interactions.

As shown in Fig. 1(b), we first placed the ice cube directly onto the CNTA and SG surfaces as close as possible but without atomic overlap. All simulations were carried using the open-source MD code, LAMMPS [44]. The equilibration of the ice-substrate systems was carried out during $0.5 \times 10^6$ MD time steps. The time step used in our simulations is 0.002 ps. The Nosé-Hoover thermostat was used to maintain the ice cube at the target temperature with the coupling time constant of 0.2 ps. After the equilibration period, the pulling force was applied on the ice cube to study its adhesion strength [see Fig. 1(c)]. In practice, we applied an acceleration field, whose magnitude increases linearly with time (t), to all oxygen and hydrogen atoms in the +z direction. The magnitude of the acceleration started at zero and increased linearly with $5.734 \times 10^{-4}$ nm · ps$^{-2}$ per MD time step. After pulling force was applied on the ice cube, the substrate responded with an attractive force on the ice cube. We monitored this attractive force ($F_A$) by collecting the force that the ice cube imposes on the substrate. Fig. 2 shows a representative example of MD simulations with the SG surface in order to explain how we obtained the detaching force ($F_D$) on the ice cube.

It can be seen in Fig. 2 that the attractive force between the ice cube and the substrate increases linearly with superimposed fluctuations and exhibits a sudden drop at the moment when the ice cube detaches completely from the substrate. In simulations, it is difficult to determine accurately $F_D$ from the fluctuating attractive force. However, the expected attractive force was also recorded by the applied acceleration on the ice cube. Therefore, we plotted both the fluctuating attractive force on the substrate (the red line in Fig. 2) and the expected attractive force (the green line in Fig. 2). As illustrated in Fig. 2, we performed a fit of the part of the fluctuating attractive force, which was significantly below the expected attractive force, using the biphasic dose-response function [45]. We then extrapolated the fitting function to the intersection with the green line depicting the expected attractive force. Thus, the coordinates of the intersection point in the $F_D - t$ plot were used to determine the detaching force and time as shown in Fig. 2(b). We found that adjusting the size of the fitting region only slightly influenced the values of the detaching force and time. Finally, the ice adhesion strength, $\sigma_D$, was calculated by normalizing $F_D$ with the ice-substrate contact area (A).

## 3. Results and discussion

### 3.1. Ice detaching from CNTA and SG surfaces

In our simulations, the pulling force on the ice cube is applied by imposing an acceleration on all oxygen and hydrogen atoms in the +z direction (perpendicular to the solid substrates). We steadily loaded the pulling force onto the whole ice cube by increasing the vertical acceleration at a constant rate. Eventually, the pulling force exceeds the maximum of the adhesion force between the ice cube and the substrate, and the ice cube will be completely detached from the substrate. The detachment event is typically associated with an abrupt drop of the adhesion force as shown in Fig. 3(a).

It has been demonstrated in the previous studies [37] that MD simulations are able to capture the ice detachment process at the atomistic level, thus providing nanoscale details of the ice detachment dynamics. As shown in Fig. 3, we first studied the ice detachment from the SG and CNTAs surfaces using the water-carbon interaction potential, which reproduces experimentally observed contact angle of water on a graphene surface [40]. The interaction parameters of the Lennard-Jones potential in this case are set $\sigma_{CO} = 3.19$Å and $\varepsilon_{CO} = 0.4736$ kJ/mol $= 0.54\varepsilon_{OO}$ For comparison, the results for the case with the smaller interaction strength, $\varepsilon_{CO} = 0.2\varepsilon_{OO}$, are also presented in Fig. 3(a) and (b).

Fig. 3(c) shows a sequence of four typical snapshots of the ice cube detaching from the CNTA surface. It can be seen from Fig. 3(c) that the pulling force first tears the ice cube at one corner from the CNTA surface. Then, the ice cube becomes more tilted relative to the substrate and finally gets ripped from the substrate. A similar detaching process of the ice cube was also observed for all cases with the CNTA and SG surfaces for different interaction energies, which is consistent with the previous MD studies [37]. Such corner-initiated detachment mechanism of the ice cube is consistent with experimental observations [46]. One plausible explanation of such detachment mechanism is that sharp edges or corners of the ice cube possess the largest pulling stress owing to their singularity [47]. Consequently, the thermal fluctuations of the ice molecules are most likely to induce the ice cube detachment from the corners.

The extensive analysis of the reduced ice adhesion on SHS [48] indicates that the low ice adhesion results from low solid/ice interfacial energy, small solid/ice contact area, and the stress concentration at the top of microposts. In the case of the CNTA surface considered in our study, the peculiar topological structure of SWNTs is characterized by very low solid/ice contact area that leads to stress localization. As expected, the ice adhesion strength on the CNTA surface is much lower than that on the SG surface [see Fig. 3(b)]. For the case $\varepsilon_{CO} = 0.54\varepsilon_{OO}$, the ice adhesion strength at the CNTA surface is 192 MPa, which is significantly lower than the value 364 MPa measured at the SG surface. In other words, the CNTA surface reduces ice adhesion strength by about 45% in comparison with the SG surface. The adhesion reduction of the CNTA surface for weaker interaction strength is even more evident. We obtained the ice adhesion strength of 54 MPa for the CNTA surface for $\varepsilon_{CO} = 0.2\varepsilon_{OO}$, which is about 50% decrease from the SG surface in the ice adhesion strength [see as in Fig. 3(b)].

In the published experimental results on anti-icing, the typical magnitude of the ice detaching strength is ~1 MPa or less [5], which is two orders of magnitude smaller than in our work and other MD simulation studies [37]. Recently, Xiao and He [37] have argued that this overestimation follows directly from the typical loading rates used in MD simulations, which are about 6–7 orders higher than in experimental studies. In particular, it was shown that the ice detaching stress increases logarithmically with the loading rate [49]. If the same loading rate were used in MD simulations and experiments, the magnitude of the ice detaching stress would be comparable between the two approaches [37]. Besides the issue with the loading rates in MD studies, the nanoscale size of the ice cube is partially responsible for the high ice detaching stress [37]. In the present study, the loading rate was kept the same in all cases. Therefore, we conclude that the reduction of the ice adhesion strength using CNTA surface is verified.

### 3.2. The correlation between the ice adhesion strength and SII energies

We next discuss the variation of the ice adhesion strength at the SG and CNTA surfaces for different oxygen-carbon interaction energies and temperatures presented in Fig. 4. It can be clearly observed that in the accessible range of energies and temperatures, the ice adhesion strength at the CNTA surface is significantly smaller than at the SG surface. Such results further confirm the reduced ice adhesion on the CNTA surface.

It is important to note in Fig. 4 that the relationship between the ice adhesion strength and the oxygen-carbon interaction energy for both CNTA and SG surfaces at a given temperature follows the linear dependence, $\sigma \sim \varepsilon_{CO}$. Such a linear relationship can be understood

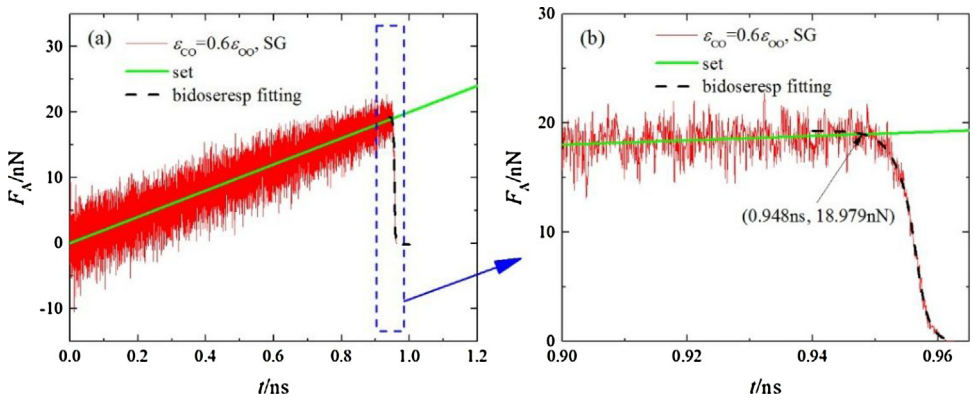


**Fig. 2.** The numerical procedure used to determine the ice adhesion strength on a solid substrate. The MD simulations were carried out for the ice cube detaching from a smooth graphene. The interaction energy between carbon and oxygen atoms is$\varepsilon_{CO}$=0.6$\varepsilon_{OO}$. (a) The solid red line is the fluctuating adhesion force between the ice cube and the solid substrate. The green line is the pulling force imposed on the ice cube as a function of time. The black dashed line is the least-square fit of the red line for the part below the green line using the bidirectional-dose-response function. (b) An enlarged view of the region enclosed by the blue dashed line in the panel (a). The ice adhesion strength was determined by the intersection between the green line and the extrapolated biphasic dose-response function. (For interpretation of the references to colour in this figure legend, the reader is referred to the web version of this article.)

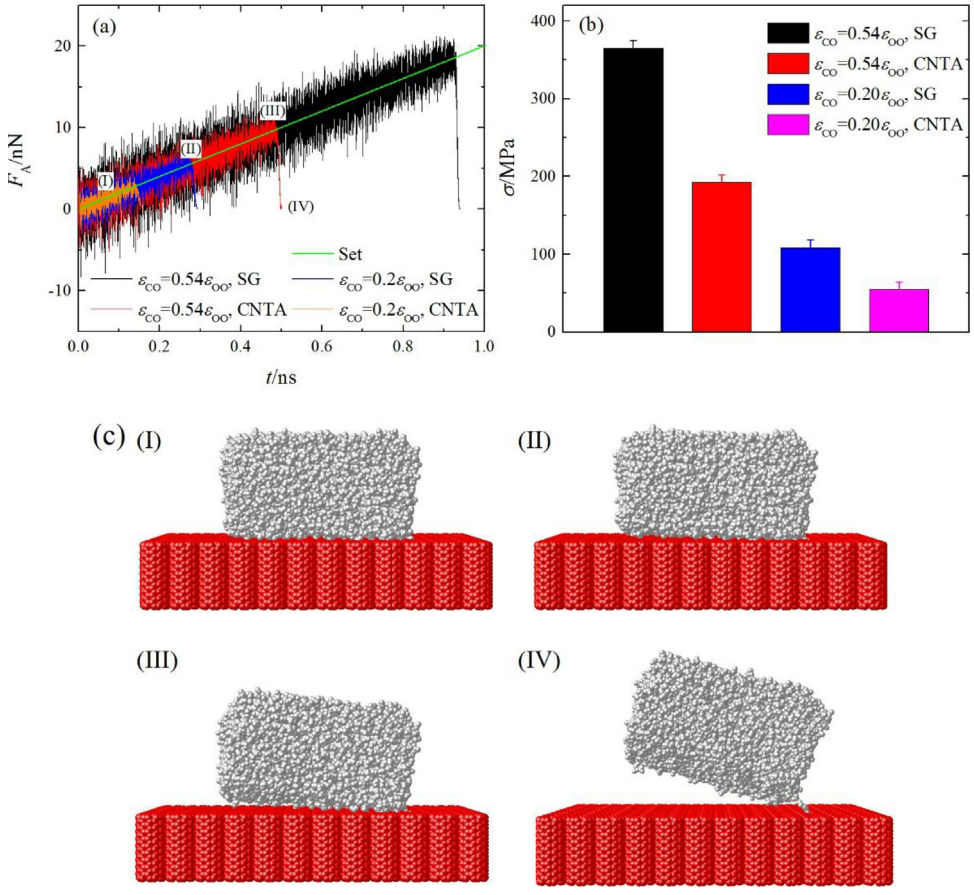


**Fig. 3.** The comparison of ice adhesion strength between the smooth graphene (SG) and the array of vertical carbon nanotubes (CNTA). (a) Time dependence of the fluctuating adhesion force during the detachment of the ice cube from the SG and CNTA surfaces. (b) The detaching stress for the indicated systems. The error bars show standard deviation from five independent runs. The color code and legends in panels (a) and (b) are the same. (c) A sequence of snapshots of the CNTA system [red curve in the panel (a)] during the ice cube detachment process. The roman numbers in the panel (a) indicate the average forces that correspond to spatial configurations shown in the panel (c). (For interpretation of the references to colour in this figure legend, the reader is referred to the web version of this article.)

by considering the influence of $\varepsilon_{CO}$ on the substrate wettability, which was shown to be directly related to the ice adhesion strength [5,13,27]. Let's first consider the case of SG surfaces. In general, the wettability of an atomically flat solid surface is controlled by the strength of interaction between the liquid and solid atoms. In our study, the liquid-solid interaction is determined by the oxygen-carbon interaction energy, $\varepsilon_{CO}$. The wettability of a solid surface is typically quantified via the contact angle ($\theta$) of a liquid droplet

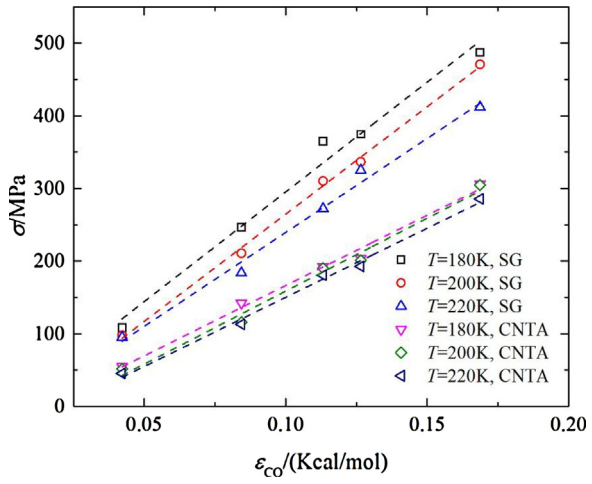


**Fig. 4.** The ice adhesion strength for the SG and CNTA versus the interaction energy between carbon and oxygen atoms, $\varepsilon_{CO}$, for different temperatures of ice, T. The dashed lines represent the best fit to the data.

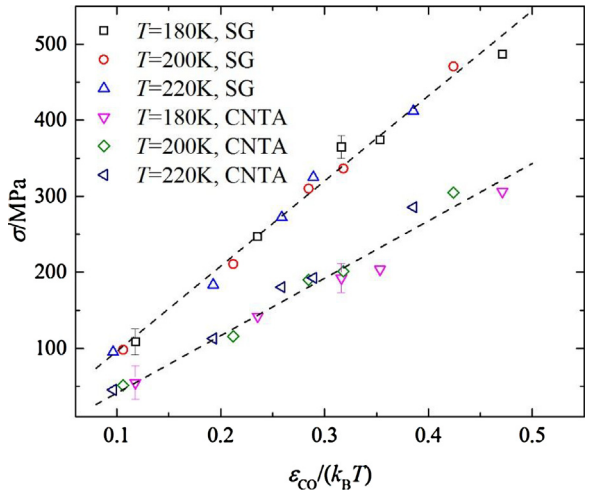


**Fig. 5.** The relationship between the ice adhesion strength and the ratio, $\varepsilon_{CO}/(k_BT)$, for the SG and CNTA systems, where $\varepsilon_{CO}$ is the interaction energy between carbon and oxygen atoms and T is the temperature of the ice cube. $k_B$ is the Boltzmann constant.

residing on the solid surface. Recently, Sendner et al. [42] deduced the linear correlation between cos $\theta$ and $\varepsilon_{CO}$ for water droplets residing on a solid substrate based on the concept of depletion layer, which is briefly summarized below.

By assuming homogeneous solid and liquid densities $\rho_S$ and $\rho_L$ and neglecting any electrostatic or interfacial entropy contributions, Sendner et al. theoretically calculated the work $H_{12}$ per surface area required to separate the liquid and solid slabs, which is defined as

$$H_{12} = \gamma_{SV} + \gamma_{LV} - \gamma_{SL} = -\pi\rho_L\rho_S \int_{z^*}^{R_0} dz z(z - z^*)^2 u(z), \quad (1)$$

where $\gamma_{SV}$, $\gamma_{LV}$ and $\gamma_{SL}$ are the values of surface tension between the solid-vapor (SV), liquid-vapor (LV) and solid-liquid (SL), respectively. Here, u(z) denotes the solid-liquid interaction energy, which in our case is modeled via the LJ interaction between the carbon and oxygen atoms. In Eq. (1), $R_0$ is the cutoff radius for the function u(z), and $z^*$ is the width of the depletion layer of water in contact with the solid surface. Clearly, since the LJ potential depends linearly on $\varepsilon_{CO}$, $H_{12}$ becomes a linear function of $\varepsilon_{CO}$ as well. Combining the above with the Young's equation, one can get the following expression

$$1 + \cos\theta = (\gamma_{SV} + \gamma_{LV} - \gamma_{SL})/(\gamma_{LV} = H_{12}/\gamma_{LV} \sim \varepsilon_{CO}. \quad (2)$$

Recent experiment studies [27] have demonstrated that the ice adhesion strength scales linearly with the cosine of the receding angle of a water droplet on a solid surface, i.e., $\sigma \sim 1 + \cos\theta_{rec}$. In our study, the atomically flat surface, i.e., the SG surface, does not exhibit the contact angle hysteresis [50], meaning that the receding angle of a water droplet is the same as the equilibrium contact angle. Therefore, the ice adhesion strength varies linearly with the cosine of the contact angle of a water droplet on a solid surface as follows

$$\sigma \sim 1 + \cos\theta. \quad (3)$$

Hence, it follows from Eqs. (2) and (3) that the ice detaching stress is a linear function of the ice-substrate interaction energy; that is, $\sigma \sim \varepsilon_{CO}$, as shown in Fig. 4.

For a smooth, chemically homogeneous surface, the contact angle, $\theta$, is called the *intrinsic* contact angle. For some structured surfaces, the water cannot fill the cavities between corrugations, and the liquid-vapor interface becomes suspended at the tops of the surface corrugations, thus forming the so-called Cassie state or fakir state. In the case of the CNTA surfaces considered in our study, the results of MD simulations indicate that water droplets always form the Cassie state for all accessible values of $\varepsilon_{CO}$. This is expected since the diameter of the SWNT and the distance between adjacent SWNTs are both very small, i.e., less than 2 nm. In the Cassie state, the surface texture leads to large values of the *apparent* contact angle. Furthermore, the contact angles of water droplets on a smooth surface and a structured surface relate as follows [5]

$$1 + \cos\theta^* = \phi_s(1 + \cos\theta), \quad (4)$$

where $\theta^*$ is the contact angle of a water droplet on a structured surface and $\phi_S$ is the solid area fraction of the solid surface in contact with the water droplet. Note that $\phi_S$ is constant in all our cases. Thus, the ice detaching stress is also a linear function of the water-surface interaction energy for the CNTA surface; namely, $\sigma \sim \phi_S\varepsilon_{CO}$. Since $\phi_S < 1$, the slope of the linear function between $\sigma$ and $\varepsilon_{CO}$ for the CNTA surface is smaller than that for the SG surface, as shown in Fig. 4.

### 3.3. The universal dependence of the ice adhesion strength on SII energy and temperature

In the process of the ice cube detachment from an atomistic substrate, the temperature of the ice cube also influences the adhesion strength along with the interaction energy between ice and substrate. Increasing temperature can enhance the mobility of water molecules of the ice cube, thus reducing the ice adhesion strength. Therefore, the temperature and the substrate-ice interaction energy have opposite effects on the ice adhesion strength. Thus, for a given substrate-ice interaction energy, higher temperature produces lower ice adhesion strength for both CNTA and SG surfaces (see Fig. 4). Furthermore, the results presented in Fig. 4 indicate that the linear correlation between the ice detaching stress and the wettability of the solid substrate also holds at different temperatures. However, such linear correlation was obtained empirically both in previous experiments and in our simulations. The rigorous explanation of this correlation will be pursued in our future studies. At a given value of the substrate-ice interaction energy, the influence of the temperature on the ice adhesion strength cannot be simply obtained. It can be seen from the Eqs. (1) and (2) that the temperature has influence both on the width of the depletion layer and the water-vapor surface tension. Therefore, the relationship between temperature and cosine of the contact angle of a water droplet on a solid surface is expected to be nontriv-

ial. Considering the competitive roles played by the temperature and the water-substrate interaction energy on the ice adhesion strength, we replotted the ice detaching stress as a function of the ratio $\varepsilon_{CO}/k_BT$ in Fig. 5. Remarkably, the correlation between the ice detaching strength and the ratio $\varepsilon_{CO}/k_BT$ can also be well described by a linear function as shown in Fig. 5. Furthermore, the slope of the linear dependence between $\sigma$ and $\varepsilon_{CO}/k_BT$ for the CNTA surface is also smaller than that for the SG surface, which is consistent with the results presented in Fig. 4.

## 4. Conclusions

In this paper, the ice detachment process from CNTA and SG surfaces was studied using all-atom molecular dynamics simulations. The pulling force on the ice cube was introduced by imposing an increasing acceleration field on the ice cube. The processes of ice detaching from the CNTA and SG surfaces are similar, i.e., the ice cube detaches starting from one of the corners under the pulling force. We demonstrated that the CNTA surface exhibits up to about 45% decrease in the ice adhesion strength in comparison with the SG surface. It was also found that with decreasing substrate-ice interaction energy, the ice adhesion strength is reduced for the CNTA surface. We observed that the ice detaching strength depends linearly on the substrate-ice interaction strength measured by the oxygen-carbon interaction energy, $\varepsilon_{CO}$, on CNTA and SG surfaces for different temperatures of the ice cube. Combining the effects of the oxygen-carbon interaction energy and the surface structure on its wettability, we proved the linear correlation between the wettability and the ice adhesion strength reported in experimental studies. Moreover, our results indicate that the MD data for the ice adhesion strength can be collapsed onto two master curves as a function of the ratio between the water-carbon interaction energy and temperature of the ice cube for the CNTA and SG surfaces. With recent advances in manufacturing CNTA surfaces, such composite systems open prospective for designing robust surfaces with low ice adhesion for passive anti-icing applications.

## Acknowledgements

This work was supported by the Natural Science Basic Research Plan in Shaanxi Province of China (Grant No. 2016JM1002) and Natural Science Basic Research Plan in Shenzhen City of China (Grant No. JCYJ20160510140747996).

## References

[1] J. Andrey, R. Olley, The relationship between weather and road safety: past and future research directions, Climatol. Bull. 24 (1990) 123–137.
[2] A.K. Andersson, C. Lee, The impact of climate change on winter road maintenance and traffic accidents in West Midlands, UK, Accid. Anal. Prev. 43 (2011) 284–289.
[3] F.R. Mosher, D. Schaum, C. Herbster, T. Guinn, Analysis of causes of icing conditions which contributed to the crash of contentental flight 3407, in: 14th Conference on Aviation, Range, and Aerospace Meteorology, Atlanta, 2010.
[4] J. Lv, Y. Song, L. Jiang, J. Wang, Bio-inspired strategies for anti-icing, ACS Nano 8 (2014) 3152–3169.
[5] M.J. Kreder, J. Alvarenga, P. Kim, J. Aizenberg, Design of anti-icing surfaces: smooth, textured or slippery? Nat. Rev. Mater. 1 (2016) 15003.
[6] P. Frohboese, A. Anders, Effects of icing on wind turbine fatigue loads, J. Phys. Conf. Ser. 75 (2007) 012061.
[7] J.L. Laforte, M.A. Allaire, J. Laflamme, State-of-the-art on power line de-icing, Atmos. Res. 46 (1998) 143–158.
[8] L.B. Boinovich, A.M. Emelyanenko, Anti-icing potential of superhydrophobic coatings, Mendeleev Commun. 23 (2013) 3–10.
[9] R.W. Gent, N.P. Dart, J.T. Cansdale, Aircraft icing, Philos. Trans. R. Soc. Lond. Ser. A Math. Phys. Eng. Sci. 358 (2000) 2873–2911.
[10] P. Zhang, F.Y. Lv, A review of the recent advances in superhydrophobic surfaces and the emerging energy-related applications, Energy 82 (2015) 1068–1087.
[11] R. Carriveau, A. Edrisy, P. Cadieux, R. Mailloux, Ice adhesion issues in renewable energy infrastructure, J. Adhes. Sci. Technol. 26 (2012) 447–461.
[12] T. Onda, S. Shibuichi, N. Satoh, K. Tsujii, Super-water-repellent fractal surfaces, Langmuir 12 (1996) 2125–2127.
[13] J.T. Simpson, S.R. Hunter, T. Aytug, Superhydrophobic materials and coatings: a review, Rep. Prog. Phys. 78 (2015) 086501.
[14] A.B.D. Cassie, S. Baxter, Wettability of porous surfaces, Trans. Faraday Soc. 40 (1944) 546–551.
[15] N. Tretyakov, M. Mueller, Correlation between surface topography and slippage, Soft Matter 9 (2012) 3613–3623.
[16] X.M. Li, D. Reinhoudt, M. Crego-Calama, What do we need for a super-hydrophobic surface? A review on the recent progress in the preparation of super-hydrophobic surfaces, Chem. Soc. Rev. 36 (2007) 1350–1368.
[17] X. Deng, L. Mammen, H.J. Butt, D. Vollmer, Candle soot as a template for a transparent robust superamphiphobic coating, Science 335 (2012) 67–70.
[18] D. Richard, D. Quéré, Bouncing water drops, EPL 50 (2000) 769–775.
[19] P. Tourkine, M.L. Merrer, D. Quéré, Delayed freezing on water repellent materials, Langmuir 25 (2009) 7214.
[20] S.A. Kulinich, M. Farzaneh, Ice adhesion on super-hydrophobic surfaces, Appl. Surf. Sci. 255 (2009) 8153–8157.
[21] L. Ge, G. Ding, H. Wang, J. Yao, P. Cheng, Y. Wang, Anti-icing property of super-hydrophobic octadecyltrichlorosilane film and its ice adhesion strength, J. Nanomater. 2013 (2013) 278936.
[22] A. Dib, A. Haiahem, B. Bou-Said, Superhydrophobic nanocomposite surface topography and ice adhesion, ACS Appl. Mater. Interfaces 6 (2014) 9272–9279.
[23] Q. Fu, X. Wu, D. Kumar, J.W.C. Ho, P.D. Kanhere, N. Srikanth, E. Liu, P. Wilson, Z. Chen, Development of sol-gel icephobic coatings: effect of surface roughness and surface energy, ACS Appl. Mater. Interfaces 6 (2015) 20685–20692.
[24] A. Ahuja, J.A. Taylor, V. Lifton, A.A. Sidorenko, T.R. Salamon, E.J. Lobaton, P. Kolodner, T.N. Krupenkin, Nanonails: a simple geometrical approach to electrically tunable superlyophobic surfaces, Langmuir 24 (2008) 9–14.
[25] A. Tuteja, W. Choi, M. Ma, J.M. Mabry, S.A. Mazzella, G.C. Rutledge, G.H. McKinley, R.E. Cohen, Designing superoleophobic surfaces, Science 318 (2007) 1618–1622.
[26] T.L. Liu, C.J. Kim, Repellent surfaces. Turning a surface superrepellent even to completely wetting liquids, Science 346 (2014) 1096–1100.
[27] A.J. Meuler, J.D. Smith, K.K. Varanasi, J.M. Mabry, G.H. Mckinley, R.E. Cohen, Relationships between water wettability and ice adhesion, ACS Appl. Mater. Interfaces 2 (2015) 3100–3110.
[28] R. Jafari, M. Farzaneh, L.F. Mobarakeh, The ice repellency of plasma polymerized HMDSO coatings, Appl. Surf. Sci. 284 (2013) 459–463.
[29] Y. Wang, J. Xue, Q. Wang, Q. Chen, J. Ding, Verification of icephobic/anti-icing properties of a superhydrophobic surface, ACS Appl. Mater. Interfaces 5 (2013) 3370–3381.
[30] S. Farhadi, M. Farzaneh, S.A. Kulinich, Anti-icing performance of superhydrophobic surfaces, Appl. Surf. Sci. 257 (2011) 6264–6269.
[31] G. Momen, R. Jafari, M. Farzaneh, Ice repellency behaviour of superhydrophobic surfaces: effects of atmospheric icing conditions and surface roughness, Appl. Surf. Sci. 349 (2015) 211–218.
[32] S.A. Kulinich, S. Farhadi, K. Nose, X.W. Du, Superhydrophobic surfaces: are they really ice-repellent? Langmuir 27 (2011) 25–29.
[33] S. Zhang, L. Kang, W. Xiao, L. Tong, L. Yang, Z. Wang, K. Qi, S. Deng, Q. Li, X. Bai, Arrays of horizontal carbon nanotubes of controlled chirality grown using designed catalysts, Nature 543 (2017) 234–238.
[34] J.L. Abascal, E. Sanz, F.R. García, C. Vega, A potential model for the study of ices and amorphous water: TIP4P/Ice, J. Chem. Phys. 122 (2005) 234511.
[35] J.P. Ryckaert, G. Ciccotti, H.J.C. Berendsen, Numerical integration of the cartesian equations of motion of a system with constraints: molecular dynamics of n-alkanes, J. Comput. Phys. 23 (1977) 327–341.
[36] C. Lobban, J.L. Finney, W.F. Kuhs, The structure of a new phase of ice, Nature 391 (1998) 268–270.
[37] S. Xiao, J. He, Z. Zhang, Nanoscale deicing by molecular dynamics simulation, Nanoscale 8 (2016) 14625–14632.
[38] Q.Z. Yuan, Y.P. Zhao, Precursor film in dynamic wetting, electrowetting, and electro-elasto-capillarity, Phys. Rev. Lett. 104 (2010) 246101.
[39] J.D. Coninck, T.D. Blake, Wetting and molecular dynamics of simple liquids, Annu. Rev. Mater. Res. 38 (2008) 1–22.
[40] B. Ramos-Alvarado, S. Kumar, G.P. Peterson, Hydrodynamic slip length as a surface property, Phys. Rev. E 93 (2016) 023101.
[41] Z. Li, Y. Wang, A. Kozbial, G. Shenoy, F. Zhou, R. McGinley, P. Ireland, B. Morganstein, A. Kunkel, S.P. Surwade, L. Li, H. Liu, Effect of airborne contaminants on the wettability of supported graphene and graphite, Nat. Mater. 12 (2013) 925–931.
[42] C. Sendner, D. Horinek, L. Bocquet, R.R. Netz, Interfacial water at hydrophobic and hydrophilic surfaces: slip, viscosity, and diffusion, Langmuir 25 (2009) 10768–10781.
[43] K. Falk, F. Sedlmeier, L. Joly, R.R. Netz, L. Bocquet, Molecular origin of fast water transport in carbon nanotube membranes: superlubricity versus curvature dependent friction, Nano Lett. 10 (2010) 4067–4073.
[44] S. Plimpton, Fast parallel algorithms for short-range molecular-dynamics, J. Comput. Phys. 117 (1995) 1–19.
[45] G.Y.D. Veroli, C. Fornari, I. Goldlust, G. Mills, S.B. Koh, J.L. Bramhall, F.M. Richards, D.I. Jodrell, An automated fitting procedure and software for dose-response curves with multiphasic features, Sci. Rep. 5 (2015) 14701.
[46] S.B. Subramanyam, K. Rykaczewski, K.K. Varanasi, Ice adhesion on lubricant-impregnated textured surfaces, Langmuir 29 (2013) 13414–13418.

[47] L.Y. Shang, Z.L. Zhang, B. Skallerud, Evaluation of fracture mechanics parameters for free edges in multi-layered structures with weak singularities, Int. J. Solids Struct. 46 (2009) 1134–1148.
[48] V. Hejazi, K. Sobolev, M. Nosonovsky, From superhydrophobicity to icephobicity: forces and interaction analysis, Sci. Rep. 3 (2013) 2194.
[49] J.K. Singh, F. Müller-Plathe, On the characterization of crystallization and ice adhesion on smooth and rough surfaces using molecular dynamics, Appl. Phys. Lett. 104 (2014) 021603.
[50] P.G. de Gennes, Wetting statics and dynamics, Rev. Mod. Phys. 57 (1985) 827–863.